Title

Kinetics of sulfide mineral oxidation in seawater: Implications for acid generation during in situ mining of seafloor hydrothermal vent deposits

Authors

Bilenker, Laura D
Romano, Gina Y
McKibben, Michael A

Peer reviewed

Kinetics of sulfide mineral oxidation in seawater: Implications for acid generation during *in situ* mining of seafloor hydrothermal vent deposits ☆

Laura D. Bilenker [*,1], Gina Y. Romano, Michael A. McKibben

Department of Earth Sciences, University of California, Riverside, CA 92521, USA

ARTICLE INFO

ABSTRACT

Growth in global metal demand has fostered a new age of unconventional mining on the seafloor. *In situ* pulverization and extraction of seafloor massive sulfide (SMS) deposits is economically attractive due to minimal overburden and high ore grades. However, important environmental questions remain on the significance of localized acid generation via irreversible sulfide mineral oxidation. Data on the reaction kinetics are necessary to estimate anthropogenic acid production during seafloor mining.

Laboratory experiments were performed to evaluate the effects of pH, temperature, dissolved oxygen, and surface area on the oxidation rate of pyrrhotite and chalcopyrite in seawater. These minerals were chosen to constrain the range of reaction rates because pyrrhotite oxidizes relatively quickly while chalcopyrite is kinetically slow. The rate laws for the abiotic oxidation of pyrrhotite and chalcopyrite in seawater at 22 °C are given in the form:

$$R_{sp} = K(m_{O2})^a(m_{H+})^b$$

where R_{sp} is the specific rate (moles m^{-2} sec^{-1}), k is the rate constant, oxygen and proton concentrations are expressed in molalities (m), and their reaction orders as a and b, respectively. The specific rate laws obtained for each sulfide studied are:

$$R_{sp(pyrrhotite)} = -10^{-7.27}\left(m_{O2(aq)}\right)^{0.51\pm0.08}(m_{H+})^{0.08\pm0.03}$$

$$R_{sp(chalcopyrite)} = -10^{-9.38}\left(m_{O2(aq)}\right)^{1.16\pm0.03}(m_{H+})^{0.36\pm0.09}$$

When used to quantitatively predict maximum acid generation rates, these rate laws indicate that acid production from *in situ* SMS mining is insufficient to exceed the buffering capacity of advecting seawater. We also calculated the residence times of crushed sulfides in seawater with low P_{O2} (0.10 atm, pH of 8, 23 °C) and find that, depending on grain size, mining waste may persist near the seafloor for years. The implications are positive in terms of slow acid production, but potentially problematic considering the potential ecological effects of an unnatural influx of particulates.

© 2016 Elsevier Ltd. All rights reserved.

☆ This paper has been recommended for acceptance by A. Danielsson.
* Corresponding author.
  E-mail address: laura.bilenker@gmail.com (L.D. Bilenker).
[1] Present address: Pacific Centre for Isotopic and Geochemical Research, Department of Earth, Ocean, Atmospheric Sciences, University of British Columbia, Vancouver, V6T 1Z4, Canada.

1. Introduction

The United Nations Department of Economic and Social Affairs (DESA) has predicted that the global population will rise above 10 billion by 2100 (Heilig et al., 2012). Although it is not impossible to

support a population that size, doing so will require significantly more natural resources, including many mineral commodities that are already becoming scarce. The oceans are a largely untapped resource for economic minerals that include base, ferro-alloy and precious metals (Rona, 2008). Rapid increases in the prices of transition metals in recent years have therefore piqued interest in the *in situ* mining of seafloor deposits of metal sulfide minerals (Hoagland et al., 2010).

Sulfide-rich hydrothermal vents known as "black smokers" were discovered in 1979 on the East Pacific Rise at 21°N (Spiess et al., 1980). Largely associated with divergent tectonic plate boundaries in oceanic crust, sulfide-rich vents, chimneys, particulate plumes, and mounds are the most obvious seafloor manifestations of effluent hydrothermal activity that is driven by the convection, heating, and chemical modification of seawater within hot oceanic crust (Fornari and Embly, 1995; Hannington et al., 2005; Mills, 1995; Von Damm, 1995). Individual chimneys can grow to up to 15 m in height, and are known as seafloor massive sulfide (SMS) deposits collectively with the surrounding chimneys, sulfide mounds, and debris. While the concentration of sulfide mineral species in SMS deposits varies at each locality, the most common constituents are Fe, Cu, Zn, and Pb sulfides. Since these elements often reach economically significant concentrations, Nautilus Minerals Inc. is in the process of developing the world's first SMS mine, Solwara 1. The deposit is located at 1600 m depth 30 km off the coast of New Ireland in the Bismarck Sea. Nautilus estimates that the mine with a footprint of 0.112 km^2 will have a life of 30 months and a maximum production of 5900 tons of ore per day with the potential to extend production up to five years pending additional discoveries. Some ore processing will take place at sea before ore is transported on shore; approximately 130,000 tons of unconsolidated, non-mineralized sediment and 115,000 tons of waste rock will be slurried back to the seabed during processing (Coffey, 2008; Boschen et al., 2013).

Our study considers two sulfides commonly found in SMS deposits; chalcopyrite ($CuFeS_2$) is of primary economic interest because it provides most of the world's Cu resources and is a valued host of precious metals (Kimball, 2013) and is abundant at the first proposed seafloor mining sites (e.g., Yeats et al., 2014). Pyrrhotite ($Fe_{1-x}S$) is a non-economic mineral, but is the dominant sulfide phase in many SMS deposits and may therefore make up a large proportion of SMS mine waste (Davis et al., 1992; Duckworth, 1998).

The excitement of a new frontier in seafloor mining has provoked numerous efforts to minimize environmental impacts and promote stewardship (e.g., Gwyther and Wright, 2008; Hoagland et al., 2010; Van Dover, 2011; International Marine Minerals Society, 2011; Baker and Beaudoin, 2013; International Seabed Authority, 2013). Proposed mining activities have focused on hydrothermally inactive areas due to the hazards of mining active vents, but there remain considerable concerns over potential environmental effects on flora and fauna whose ecology is recently-recognized and incompletely known (Halfar and Fujita, 2002, 2007; Drew, 2009; Van Dover, 2011; Craw, 2013). Total loss of organisms in the mining area and their disturbance in more distal areas by sedimentation of mining particulates are of the greatest concern.

In terrestrial settings, exposure of mined sulfide ores or sulfide-bearing coals to moist air or oxygenated waters can quickly oxidize the sulfide minerals, releasing sulfuric acid and solubilizing toxic elements into poorly-buffered surface and ground waters (Hoffert, 1947; Johnson, 2003; Blodau, 2006). On the ocean floor, it can be argued that the high buffer capacity and low oxygen solubility of cold seawater should act to reduce the marine equivalent of acid mine drainage (AMD) from exploited SMS deposits, and in fact much of the ochre that develops as SMS deposits naturally weather is a manifestation of this chemical neutralization process occurring slowly over geologic time (Mills and Elderfield, 1995; Edwards et al., 2003; Hrischeva and Scott, 2007).

However, *in situ* deep-sea mining of SMS deposits may still produce circumstances that are far more conducive to rapid acid generation than is first assumed when compared to terrestrial mining settings. One proposed mining strategy is to pulverize the chimneys and mounds *in situ* using remotely operated vehicles to allow the ore to be quickly and economically slurried in pipelines to surface processing ships (Gwyther and Wright, 2008; Drew, 2009; Baker and Beaudoin, 2013). Consequently, the fresh pulverized sulfide mineral grains will have extremely high specific surface areas and be entrained in an environment of high seawater advection both at the mining site and during transport to the warmer surface conditions. All of these factors promote more rapid oxidation compared to natural weathering rates on the seafloor. In addition, processing wastes such as the finest (≤8 µm) non-settling grains and non-economic sulfide minerals (e.g., pyrrhotite) will be released via return pipeline directly above the seafloor in another highly advective environment (0.3 m^3/s). If the rate of particle oxidation and sulfuric acid release is rapid enough in such settings to temporarily exceed the buffer capacity of seawater, then ecologic effects caused by increased acidity cannot be ruled out.

Whether biological processes will catalyze sulfide mineral oxidation reactions during SMS mining is another important consideration. Vent macrofauna such as grazing shrimp feed by scraping sulfide mineral surfaces (Van Dover et al., 1988; Polz et al., 1998), enhancing oxidation rates. Field incubation experiments in which fresh sulfide mineral surfaces were exposed near vent sites for two months resulted in rapid colonization of the surfaces by Fe-oxidizing bacteria (Edwards et al., 2003). Use of bacteria in terrestrial bioleaching of chalcopyrite indicates that after several days under highly acidic conditions, the biotic rate is much faster than the abiotic rate (Sasaki et al., 2009). However, under neutral to alkaline pH conditions, bacteria do not significantly catalyze sulfide mineral oxidation rates to values above abiotic rates (Schippers, 2004). Moreover, in the seafloor mining scenarios outlined above, the transit time between *in situ* pulverization, surface processing, and waste return to the seafloor is < 30 min, an insufficient amount of time to allow significant bacterial colonization of the grain surfaces and biotic catalysis of oxidation. For this reason, inorganic processes, not organic, mediate the oxidation reactions most likely to increase seawater acidity during SMS mining.
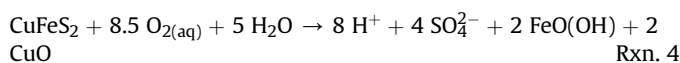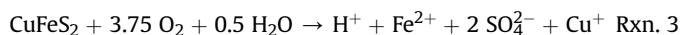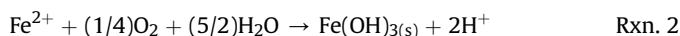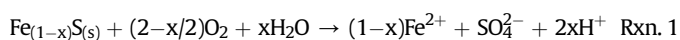
2. Previous experimental work

Laboratory-based experiments are necessary to quantify maximum sulfide mineral oxidation rates because *in situ* measurements can be difficult to make and interpret. For example, Avery and Benning (2008) measured *in situ* single grain pyrite oxidation rates under low pH vent-proximal seafloor conditions based on volumetric changes (from vertical scanning interferometry), concluding that *in situ* rates are far less rapid than stirred laboratory batch reactor rates for pyrite oxidation (McKibben and Barnes, 1986). However, they did not measure ambient fluid flow rates or otherwise evaluate if they measured transport-controlled *apparent* reaction rates (limited by oxidant diffusion or advection) rather than the maximum surface-reaction-controlled batch rates as measured in the laboratory. Laboratory kinetic experiments typically seek to measure the surface-controlled reaction rate in the absence of any fluid transport limitations, because that is the rate attributable to the nature of the specific mineral species' surface properties. Transport control on reaction rates can then be incorporated during computer modeling, which couples the laboratory-based rate laws with fluid advection and diffusion constraints (Bethke, 2008; Brantley et al., 2008). The high flow-rate laboratory

experiments are therefore more pertinent to highly advective SMS mining conditions, and will predict the *maximum* possible rate of anthropogenic acid production as needed for environmental impact assessment.

Quantifying the inorganic oxidation rates of the pertinent minerals is therefore an essential first step to understanding the potential anthropogenic impacts of SMS mining. There are no rate laws published for the oxidation kinetics of common sulfide minerals in seawater. For this study, pyrrhotite was chosen because it is a major non-economic component of SMS deposits that will be disposed of on or above the seafloor during mining (Gwyther and Wright, 2008), and chalcopyrite because it is the chief economic ore of Cu and Au in SMS deposits.

Prior studies have focused on chalcopyrite and pyrrhotite oxidation in terrestrial settings, mainly applicable to AMD (e.g., Kim et al., 1982; Pratt et al., 1994; Janzen et al., 2000; Belzile et al., 2004; Kimball et al., 2010). Both minerals oxidize irreversibly, producing sulfuric acid as well as dissolved Fe ± Cu. For example:

$$Fe_{(1-x)}S_{(s)} + (2-x/2)O_2 + xH_2O \rightarrow (1-x)Fe^{2+} + SO_4^{2-} + 2xH^+ \quad \text{Rxn. 1}$$

$$Fe^{2+} + (1/4)O_2 + (5/2)H_2O \rightarrow Fe(OH)_{3(s)} + 2H^+ \quad \text{Rxn. 2}$$

$$CuFeS_2 + 3.75\ O_2 + 0.5\ H_2O \rightarrow H^+ + Fe^{2+} + 2\ SO_4^{2-} + Cu^+ \quad \text{Rxn. 3}$$

$$CuFeS_2 + 8.5\ O_{2(aq)} + 5\ H_2O \rightarrow 8\ H^+ + 4\ SO_4^{2-} + 2\ FeO(OH) + 2\ CuO \quad \text{Rxn. 4}$$

Based on rates of Fe^{2+} release, the mean oxidation rate of pyrrhotite by dissolved oxygen (DO) is 4×10^{-9} mol m^{-2} s^{-1} at temperatures 25–45 °C and pH 2–3, for grain sizes of 125–180 μm (Janzen et al., 2000). Nicholson and Sharer (1994) report the oxidation rate of pyrrhotite to be $6{-}14 \times 10^{-9}$ mol m^{-2} s^{-1} at 22 °C from pH 2–6 for grain sizes of 105 μm; the reaction was not strongly pH dependent. A preferential retention of S on pyrrhotite grain surfaces was inferred with an increase in pH, due to an observed decrease in the molar ratio of SO_4^{2-} to Fe with increasing pH in the effluent. Total dissolved Fe was a good indicator of the oxidation rate, however at pH > 4 a chelating agent, ethylenediaminetetra acetic acid (EDTA), was used to prevent the oxidation and precipitation of Fe^{2+}. Both Fe hydroxide precipitation and the use of a chelating agent could give an erroneously low apparent rate of reaction.

Some researchers have also examined the effect of chlorine ions on the dissolution rates of chalcopyrite during ore processing in highly acid solutions (Lu et al., 2000; Ruiz et al., 2011), finding that higher Cl^- concentrations accelerate the rate. It is also important to note that in the presence of seawater, observations of atacamite $(CuCl(OH)_3)$ formation from the weathering of Cu–Fe sulfides have been reported (Hannington, 1993), the presence of which may hinder dissolution. So far, though, no experimental kinetic work on aqueous oxidative pyrrhotite or chalcopyrite dissolution in seawater has been completed (Kimball et al., 2010).

3. Experimental setting

3.1. Mineral selection and preparation

Ore samples containing large (>2 cm), nearly pure sulfide crystals were broken, crushed, and sorted under a 10–25x binocular scope to minimize impurities, then sieved to desired grain size fractions. The pyrrhotite ore came from the Dal N'gorsk Primorsky Kray Mine, Far Eastern Region, Russia and the chalcopyrite ore came from the Casapalca Mine, Huarochiri Province, Peru. Powder X-ray diffraction (XRD) confirmed the identity and integrity of both

minerals and revealed the pyrrhotite to be monoclinic. Mineral composition and purity were confirmed by using Energy Dispersive Spectroscopy (EDS) on a Philips XL30-FEG Scanning Electron Microscope (SEM).

The grain diameter size fractions of 45–106 μm and 106–150 μm were used, chosen based on optimal run duration in prior sulfide kinetics research (McKibben and Barnes, 1986; McKibben et al., 2008). To avoid erroneously high specific surface areas and initial dissolution rates that could be caused by fine powders adhering to the fresh mineral surfaces after crushing, and to remove any surface oxidation layer formed in air before the runs, grains were cleaned mechanically (ultrasonication) and chemically (dilute HCl soak and ethanol rinse) immediately before experimentation. SEM images (Fig. 1) compare pyrrhotite grains immediately after being crushed to those free of particles after cleaning.

Quantifying the surface area per mass of the mineral grains used in the experiments is necessary to derive a specific rate law (moles m^{-1} s^{-1}) for oxidation. In any fluid-mineral reaction, more available total mineral surface will result in a faster reaction, so normalizing the rate per unit surface area makes the derived rate law theoretically scalable to any grain size. The B.E.T. gas adsorption method was used to determine the specific surface area (m^2 g^{-1}) of the sized mineral grains (Brunauer et al., 1938; Fagurland, 1973). Three-point krypton gas analysis by Quantachrome Instruments yielded the surface areas for pyrrhotite of 0.119 m^2 g^{-1} and 0.033 m^2 g^{-1} for grain size fractions of 45–106 μm and 106–150 μm, respectively. Chalcopyrite grain size fractions 45–106 μm and 106–150 μm had surface areas of 0.062 m^2 g^{-1} and 0.032 m^2 g^{-1}, respectively.

3.2. Experimental design

There are two basic experimental approaches using reactors (Brantley et al., 2008; Rimstidt, 2014): batch and flow-through modes. Batch mode, in which a fixed volume of solution is stirred within a reactor, was used for the experiments reported here (Bilenker, 2011; Romano, 2012). Reaction progress was monitored through Cu and Fe concentration changes over time by analyzing samples of the experimental solution.

The batch reactor setup was similar to McKibben and Barnes (1986) and McKibben et al. (2008) (Fig. 2). The synthetic seawater used in chalcopyrite runs was prepared by using commercial aquarium salt and 18.2 MΩ water in proportions akin to natural seawater. Consistency in salinity between batches was attempted by always adding 34 g aquarium salt per liter of solution for every run. For pyrrhotite runs, synthetic seawater was instead made following the formulation of Millero (2002). Dry salts were added by gram molar mass and hygroscopic salts were added volumetrically. The Millero recipe was a more consistent formulation over the commercial aquarium salts and is recommended in future experiments. For both seawater methods, pH was adjusted with HCl and measured with a Thermo Scientific Orion 911600 Semi-Micro pH gel electrode, designed for use in saline solutions.

Prior to the start of each run, the synthetic seawater was purged with either pure O_2 or a known mixture of O_2 and N_2 to maintain a fixed DO. Seawater was also thermally equilibrated before placing mineral grains in the reactor. Cleaned grains were held between two pieces of 30 μm nylon mesh within a PVC sample platform. The sample platform was suspended by vertical plexiglass fins fitted inside the middle of a 2 L Savillex Teflon reaction vessel, which has ports in the lid for sampling, a thermometer, gas inflow, water inflow and outflow for closed-loop seawater circulation (Fig. 2). Vessels were placed inside temperature-controlled circulation baths (water-ethylene glycol) for the duration of the experiment.

To insure adequate fluid flow velocity and surface-reaction control of oxidation rates within the vessel, the seawater was
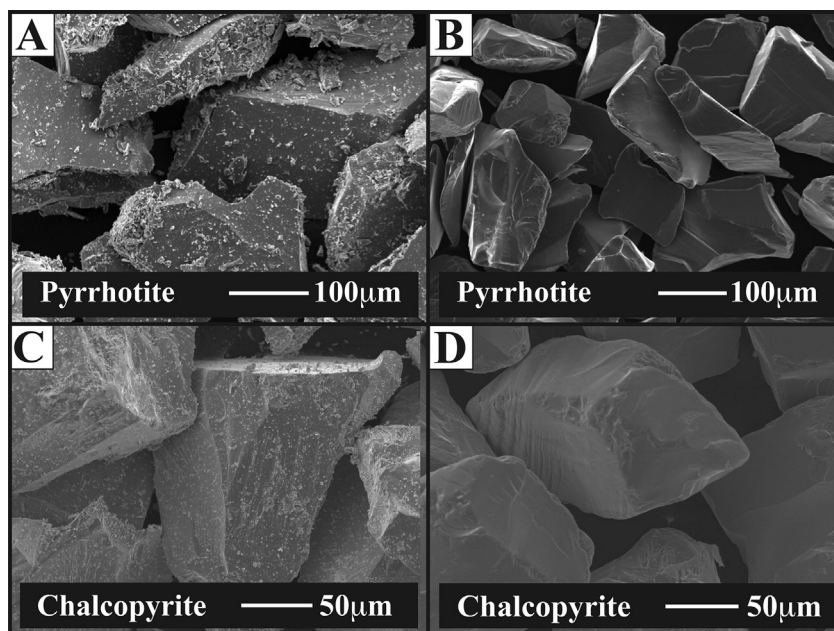
Fig. 1. SEM images of (A) pyrrhotite grains after crushing and sieving; (B) pyrrhotite grains after cleaning, before experimentation.
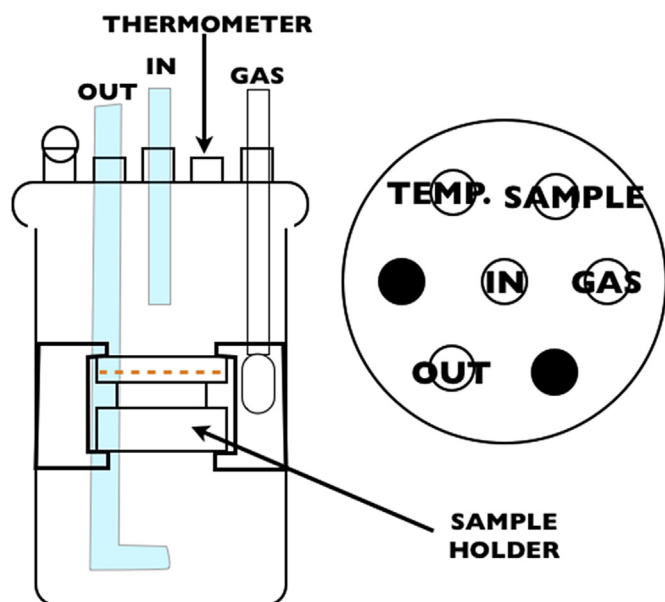

Fig. 2. On left: schematic cross section of the reaction vessel including positions of tubes and ports relative to the mineral sample (dashed orange line), based on McKibben et al. (2008). On right: map view of lid, displaying the ports (black—remained capped). The fluid sampling port was covered between extractions by a hollow Teflon ball, visible in the vessel cross section as a circle on top of the left-most port. (For interpretation of the references to colour in this figure legend, the reader is referred to the web version of this article.)

rapidly circulated through a closed peristaltic pump loop rather than by using a magnetic stirring device inside the vessel. Tracer dye tests indicated that at a pump rate of approximately 1050 mL/min, the fluid inside the vessel was completely homogenized within 31 s. Variation in the pump speed for different runs had no effect on the reaction rate under otherwise constant T-pH-DO conditions, indicating that the measured rate was fully surface-reaction controlled and not transport-limited.

Fluid samples were extracted by a fixed-volume micropipette at intervals throughout each run, always more frequently in the beginning. Only 1 mL was removed from the run for each sample aliquot, resulting in minimal seawater volume change over the lifetime of a run. Pyrrhotite runs lasted for roughly 8 h and 1 mL samples were collected every 30 min. Due to slower reaction rates, chalcopyrite runs lasted up to 72 h and samples were collected every few hours. Temperature was continuously monitored and pH was measured at the beginning and conclusion of each experiment.

During runs performed in batch mode, precipitates may accumulate in solution or as coatings on the mineral surfaces because the seawater containing dissolved reaction products is not evacuating the vessel to be replaced with fresh matrix as it would in a flow-through reactor setup. Therefore, batch mode is best suited to studying initial rates of reactions on fresh grain surfaces (Lasaga, 1998; McKibben and Barnes, 1986; McKibben et al., 2008). The SEM was also used after runs to check for surface precipitates as well as changes in surface topology.

Rate dependence on DO was determined by performing a series of runs with O_2 mixed with N_2 at different P_{O2} values (0.995 atm, 0.100 atm, and 0.010 atm) at 25 °C and pH of 3. While DO is low in seafloor settings, these three values were chosen due to available gas mixtures. To assess the effect of temperature, runs were conducted between 4 °C and 35 °C; use of temperatures above this upper limit produces rapid evaporation of water from the reaction vessels, which affects the measured concentrations by significantly altering the volume of fluid available to react with the sample. This upper temperature limit is realistic in the context of seafloor mining since environments hotter than 35 °C present a risk to the equipment (Boschen et al., 2013). Natural seafloor conditions at depths of target inactive vents at (1000–5,000 m) vary from 2 to 4 °C (Becker and Davis, 2004; Davis and Elderfield, 2004). Although the temperature range used represents the practical experimental limits of the equipment, rates at slightly lower and higher temperatures can be extrapolated by linear Arrhenius regression of the rate data with inverse temperature.

4. Analytical methods

To measure Fe and Cu concentrations in samples obtained over the course of all experiments, fluid samples were diluted ten-fold

with 2% ultrapure HNO_3 and analyzed by using an Agilent 7500 Series Inductively Coupled Plasma Mass Spectrometer (ICP-MS). The ten-fold dilution was necessary to avoid introducing potentially damaging saline fluids into the ICP-MS. Standards containing known Fe and Cu concentrations and trace metal grade 2% HNO_3 were analyzed alongside the experimental run products, in addition to a matrix control sample of ten-fold diluted synthetic seawater, which was unreacted with sulfides. The Fe and Cu counts obtained by measuring this matrix blank were then subtracted from the sample counts to yield final concentrations.

4.1. Rate law derivation

Our kinetic experiments sought to derive a rate law in the following way. For the irreversible reaction:

$$aA + bB \rightarrow cC + dD \quad (1)$$

The rate of reaction is defined as:

$$Rate = (-1/a)(dC_A/dt) = (-1/b)(dC_B/dt) = (1/c)(dC_C/dt)$$
$$= (1/d)(dC_D/dt) \quad (2)$$

which can be expressed as the rate law:

$$Rate = kC_A^{nA}C_B^{nB}C_C^{nC}C_D^{nD} \quad (3)$$

where C is concentration, reaction order n is any real number, and k is the rate constant (Lasaga, 1998). Rate and concentration are experimentally-measurable variables while the rate constant and reaction orders are the unknown parameters. The latter can be determined experimentally by the isolation method (McKibben and Barnes, 1986; Laidler, 1987; McKibben et al., 2008), in which all but one variable are held constant and its effect on the rate is quantified.

Based on prior studies in terrestrial settings we can expect that the experimental rate for the oxidation of chalcopyrite by DO in seawater within a reaction vessel will be primarily dependent on temperature, pH, salinity, and DO, having a mathematical form similar to:

$$dm_{chalcopyrite}/dt = k\,(m_{O2,aq})^a\,(m_{H+})^b\,(m_{Cl-})^c \quad (4)$$

where k is a function of temperature. We can determine the reaction order value of a manipulated variable by taking the log of the rate law:

$$\log dm_{chalcopyrite}/dt = \log\left[k\,(m_{O2,aq})^a\,(m_{Cl-})^c\right] + b\log\,(m_{H+}) \quad (5)$$

This produces the equation for a straight line on a plot of log reaction rate versus log m_{H+} whose slope equals b. All variables in the rate law can be experimentally isolated and their reaction orders determined, as can the dependence of k on temperature. Fifteen runs were used in the calculation of the rate law for pyrrhotite; sixteen runs were used in the rate law calculation for chalcopyrite.

4.2. Rate-determining variables and derivation of the initial rate

Due to a high background concentration of sulfate naturally present in seawater, total dissolved Fe or Cu were used as the rate-determining variables. If one product element (Fe or Cu)

precipitated, i.e., formed a stain on the mesh or clouded the reactor or pump tubing, the other element was used. Copper was selected as the rate-determining variable for chalcopyrite, while Fe was always used for pyrrhotite runs.

Following the differential method (Lasaga, 1998) for each run, a second-order polynomial in the form $M_i = x + yt + zt^2$ was fit to the individual run data for total dissolved Fe or Cu per unit time using the program SigmaPlot™. The slope of the second-order polynomial is found at $t = 0$ by taking the first derivative of M. This is the initial reaction rate.

5. Results

5.1. Reaction stoichiometry

All pyrrhotite experiments produced measurable dissolved Fe; as oxidation progressed, total dissolved Fe increased (Fig. 3). However, the dissolution of chalcopyrite was not stoichiometric under all conditions. The reaction did behave congruently when pH < 4.0, P_{O2} was low, and/or the temperature was $\leq 10\,°C$ (Fig. 4). Therefore, only runs performed under such conditions were used to derive the rate law. The reproducibility of data for both sulfides is shown in Fig. 3.

Measuring rates at higher pH is possible, but would require using a mixed flow reactor. In such an experimental set up, seawater would be moved through the reactor containing the mineral, but carried into an external container while new, unreacted seawater was introduced. This would prevent the formation of precipitates because the solution interacting with the mineral would not reach saturation with any phase, as it would be circulated out of the reactor. However, the effluent volumes generated by such a reactor method are large, and the resulting concentrations levels of Cu and Fe in the accumulated effluent are quite low, making rate determinations problematic.

5.2. Effect of oxidant concentration on reaction rates

Seawater has a low capacity for oxygen absorption due to the salting out effect (Benson and Krause, 1984). Dissolved oxygen (C_o^* in eq. (6)) is calculated from P_{O2} by using the following equation from Garcia and Gordon (1992), simplified from Benson and Krause (1984):

$$C_o^* = 0.20946F\,(1 - Pwv)\,(1 - Bo)\,(KoMw)^{-1} \quad (6)$$

where 0.20946 is the mole fraction of O_2 in dry air (which will be substituted with experimental values of P_{O2}), F is the salinity factor (F = 35 after Millero, 2002), P_{wv} is the vapor pressure of water in air, B_o is the second virial coefficient for O_2 (Benson and Krause, 1980), K_o is Henry's law coefficient for O_2 in seawater, and M_w is the molecular mass of water.

Increasing DO has a positive effect on the rate of oxidation (Fig. 5). However, the difference between 0.100 atm and 0.995 atm P_{O2} was not nearly as significant as the difference between 0.010 atm and 0.100 atm O_2. Linear regression of the data yields a slope of 0.51 ± 0.08 for pyrrhotite and 1.16 ± 0.03 for chalcopyrite (Fig. 5).

DO is also dependent on the density of seawater, which is affected by pressure. DO calculations were completed for a seawater density of 1.025 kg/dm^3 for surface seawater, and 1.050 kg/dm^3 for seawater at 1500 m depth. The minor change in seawater density had little effect on calculated DO, implying that pressure is a negligible factor in such oxidation rates.
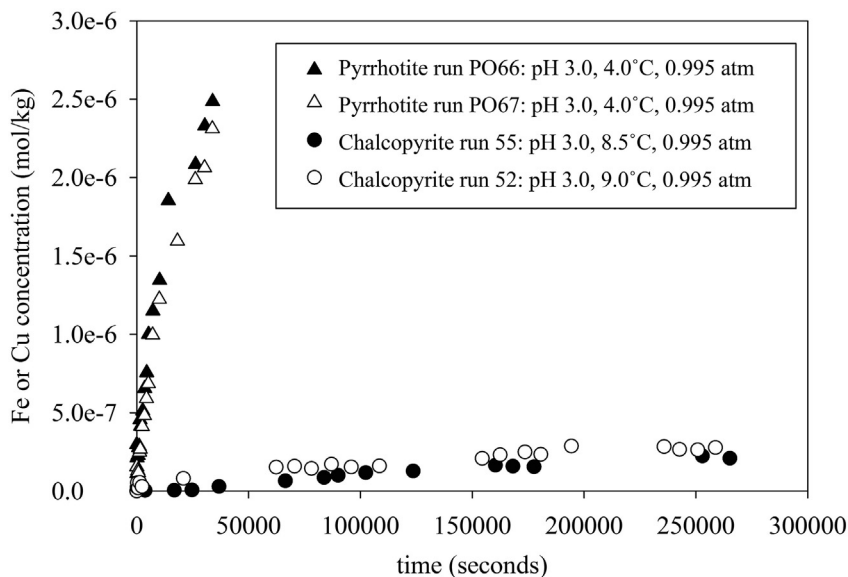
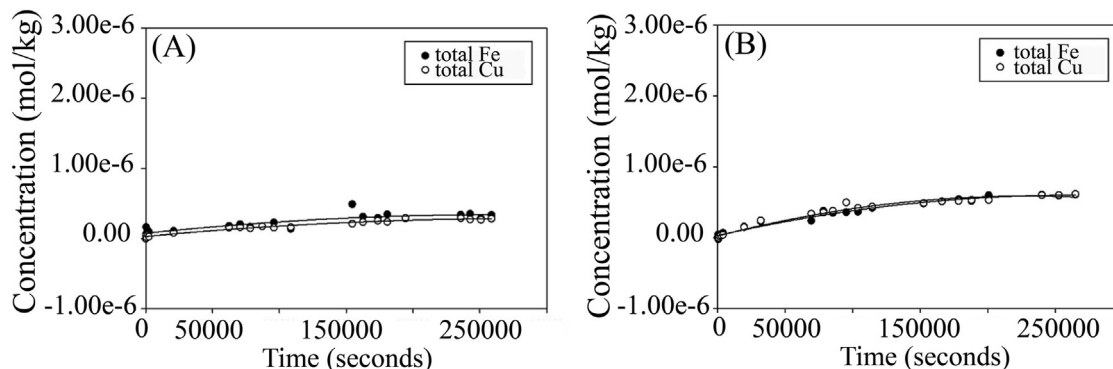**Fig. 3.** Demonstration of data reproducibility for typical pyrrhotite and chalcopyrite experiments.

Fig. 4. Plots showing conditions under which the release of dissolved Cu and Fe was stoichiometric during chalcopyrite oxidation runs. (A) Cold (9.0 °C, 0.995 atm) and (B) low P_{O2} (0.10 atm, 21.0 °C) conditions at pH = 3.0. The values reported here reflect data from which the blank seawater matrix was subtracted.

5.3. The effect of pH on reaction rates

In order to assess rate dependence on pH, runs were performed while varying the initial proton concentration at ~25 °C and P_{O2} = 0.995 atm. Iron and Cu were released more slowly into solution with less acidity from pH 2.0 to 4.0 in pyrrhotite and chalcopyrite experiments, respectively, and no significant changes in pH were observed during runs at pH ≤ 4. This is not surprising because at low pH, a large amount of released protons is required to produce a measurable change. Runs above pH of 4 resulted in irregular metal concentrations and occasional visible precipitates (staining) for both pyrrhotite and chalcopyrite. For both minerals, the dependence of the measured oxidation rate on experimental pH is shown in Fig. 6. The slope of the line in Fig. 6 is 0.08 ± 0.03 for pyrrhotite and 0.36 ± 0.09 for chalcopyrite, although in the case of pyrrhotite, perhaps it could be argued that the pH-dependence from pH 3–4 is strong while that from pH 2–3 is weak.

5.4. Formation of precipitates and thermodynamic modeling

Higher pH conditions are ideal for mine sites of inactive vents due to the limitations of the equipment, however, above a pH of ~4.0, the release of Fe from both minerals was hindered by the production of Fe–OH precipitates. Therefore, in order to quantify the simplified, "worst-case" rates of sulfide dissolution, batch runs at P_{O2} = 0.995 atm were performed at low pH to avoid precipitation of Cu and Fe hydroxides and chlorides. During chalcopyrite runs at a pH of 8.2 a fine grained, gray-white material developed on the mesh and inner walls of the pump tubing after about one day and plots of Cu and Fe concentrations over time show that neither Cu nor Fe appear to remain in solution as ions or free-floating precipitates and the initial release rates of both metals were essentially zero. In an effort to suppress precipitation long enough to obtain a usable rate at higher pH values, a few pyrrhotite runs were performed under a lower P_{O2} by using a 10% O_2 gas mixture balanced with N_2. Pyrrhotite runs at pH = 8 also generated precipitates white in color, and occasionally there was red Fe staining observed on the mesh of the sample platform. The chemical composition of the precipitates could not be identified due to an insufficient mass of material to analyze by XRD, and SEM analyses confirmed the presence of Fe. This is consistent with thermodynamic reaction progress modeling with Geochemist's Workbench (GWB), which predicts Fe hydroxide precipitation early in the reaction at seawater pH values, followed ultimately by jarosite precipitation as the pyrrhotite is completely consumed (reaction progress 1.0) (Fig. 7). Further discussion of the GWB model are provided below, in section 6.4.
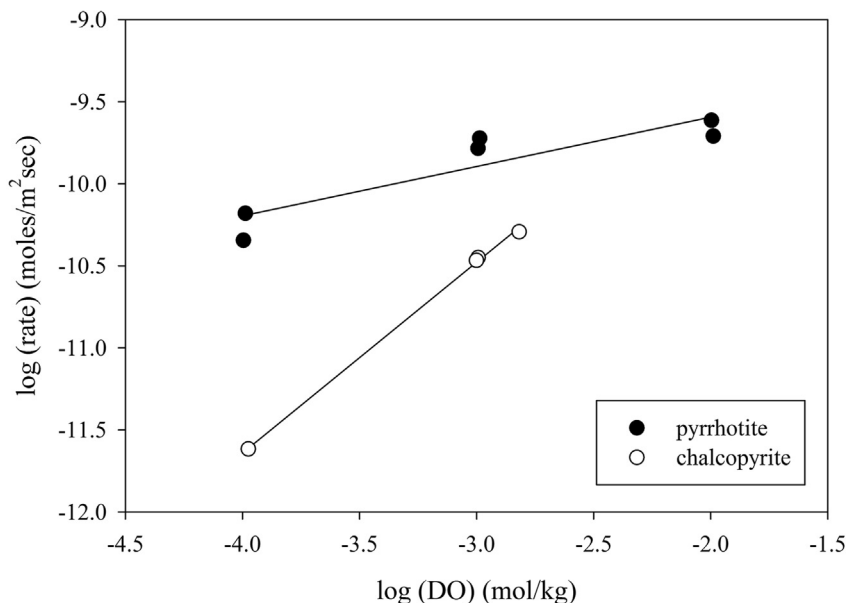
Fig. 5. Rate dependence on dissolved oxygen for pyrrhotite (solid circles) and chalcopyrite (open circles).
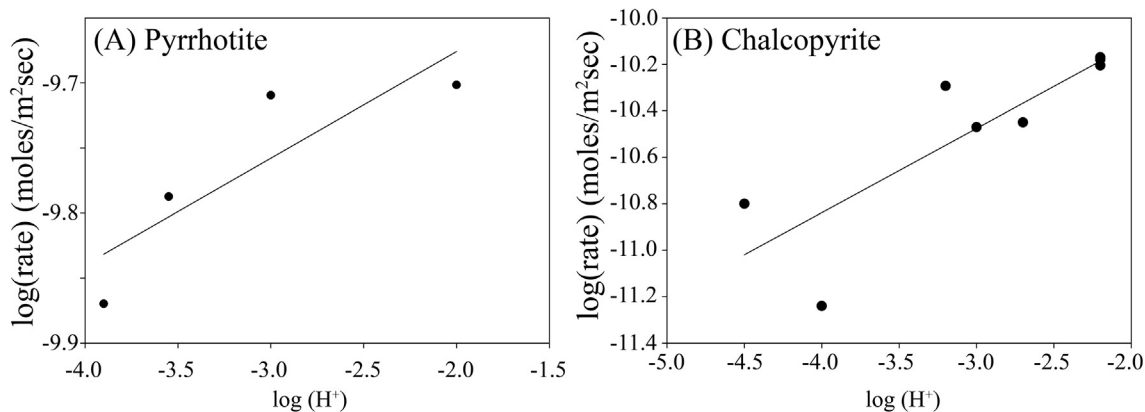

Fig. 6. Rate dependence of (A) pyrrhotite and (B) chalcopyrite oxidation on pH.

GWB also predicts that starting at a seawater pH of 7.5, the complete oxidation of 1 g of pyrrhotite in 1.8 L of seawater eventually produces enough protons to bring the final pH below 3 (Fig. 8). However, none of our runs were conducted to completion (weeks or months), so the precipitation of jarosite would not have occurred and the pH was not observed to drop so low. In fact, the actual runs conducted at initial seawater pH did not show an expected decrease in pH after 8 h, but rather a slight increase up to pH 8.5, indicating that some other unexpected reaction is taking place, or precipitates form during pyrrhotite oxidation and prevent significant further solubilization of Fe.

Modeling of the consequences of chalcopyrite oxidation by GWB could not be accomplished because there are no thermodynamic data available for atacamite, one of the expected reaction products.

5.5. Derivation of volumetric rate laws

By combining the dependencies on oxygen and proton molality determined above, the volumetric rate laws now can be written as follows:

$$R_{vol} = -k \, A/V (m_{O2})^a (m_{H+})^b \tag{7}$$

$$R_{vol(pyrrhotite)} = -k \, A/V \, (m_{O2(aq)})^{0.51\pm0.08} (m_{H+})^{0.08\pm0.03} \tag{8}$$

$$R_{vol(chalcopyrite)} = -k \, A/V \, (m_{O2(aq)})^{1.16\pm0.03} \, (m_{H+})^{0.36\pm0.09} \tag{9}$$

5.6. Effect of surface area

Experiments varying the grain size fraction showed that the reaction rates are also dependent on grain size. For a given total mass of sulfide, grains with higher specific surface area (smaller diameter) oxidize more quickly than those with lower specific surface area, which indicates a positive surface area influence on the rate. This is demonstrated most clearly for pyrrhotite (Fig. 9), where runs performed with grains of the smaller size fraction had initial rates approximately 1.74 times faster than those conducted using the larger size fraction. The slope in Fig. 9 is ~0.5, suggesting that the rate for pyrrhotite is not linear with respect to specific surface area over the grain size range that was utilized.

In comparison, the low-surface area fraction of chalcopyrite grains (106 μm−150 μm) did not provide a discernible rate that
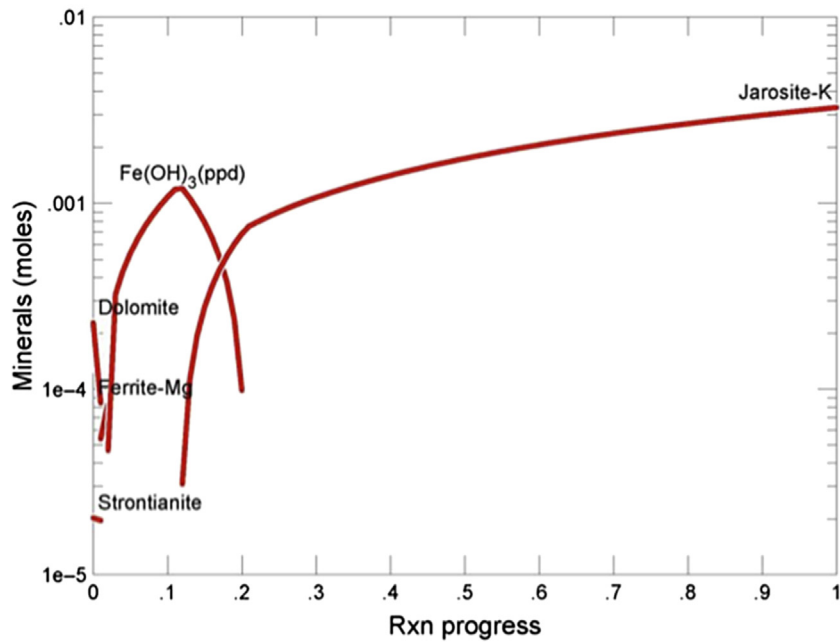
Fig. 7. Geochemist's Workbench model reacting pH 7.5 seawater with 1 g of pyrrhotite at 20.0 °C where P_{O2} = 0.995 atm.
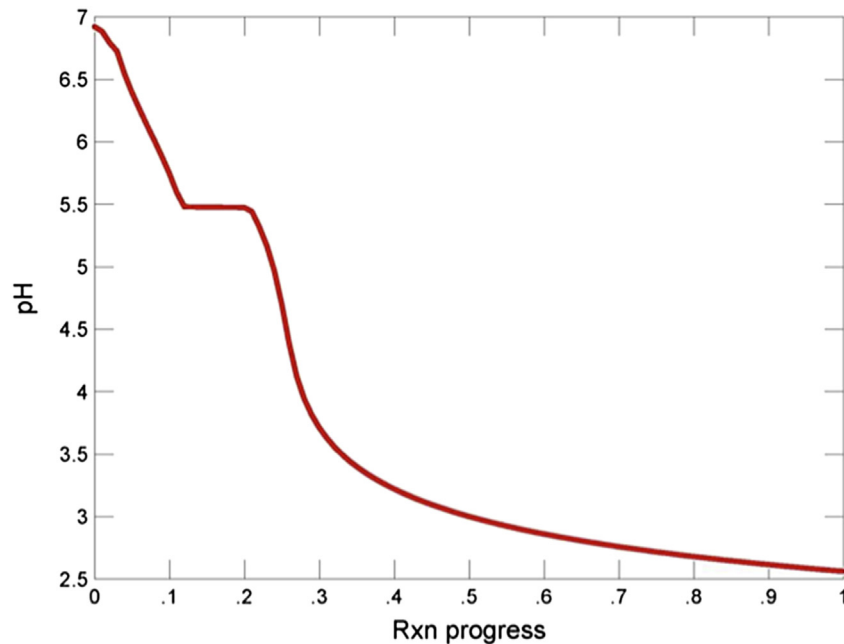

Fig. 8. Changes in pH during the complete stoichiometric oxidation of 1 g of pyrrhotite in 1 kg of seawater at 2 °C, as predicted by Geochemist's Workbench. The plateau at pH 5.5 corresponds to the dissolution of precipitated Fe hydroxide shown in Fig. 7. The initial rate experimental conditions correspond to less than 0.1 reaction progress here and in Fig. 7.

could be used with confidence. Generating grain sizes smaller than 45 μm to produce more available reactive surface (and thus more detectable rates) for chalcopyrite was not possible with the available equipment, so most of the chalcopyrite runs involved grains 45–106 μm in diameter. Using nylon screens with mesh any smaller than the 30 μm design would have inhibited the fluid throughput, producing transport-limited data. For this same reason, we were also limited to investigating just two grain size fractions for pyrrhotite.

5.7. Derivation of the specific rate law

With these surface area data, we can now derive the specific rate law (Eq. (11)) by multiplying the volumetric rate law (Eq. (7)) by V/A, where V is the volume of seawater, A is total mineral surface area, and a and b are reaction orders for the molal aqueous species; concentrations (m):

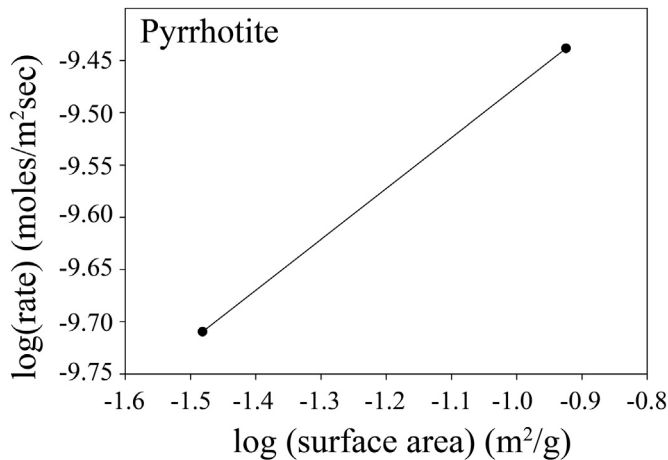$$-dM_{mineral}/\, dt = k\, (A/V)\, (m_{O2})^a\, (m_{H+})^b \tag{10}$$

Fig. 9. Rate dependence of pyrrhotite dissolution on surface area.

$$R_{sp} = k \, (m_{O2})^a \, (m_{H+})^b \tag{11}$$

The resulting specific rate laws are:

$$R_{sp(pyrrhotite)} = -k \left(m_{O2(aq)} \right)^{0.51 \pm 0.08} (m_{H+})^{0.08 \pm 0.03} \tag{12}$$

$$R_{sp(chalcopyrite)} = -k \left(m_{O2(aq)} \right)^{1.16 \pm 0.03} (m_{H+})^{0.36 \pm 0.09} \tag{13}$$

5.8. Temperature effect on reaction rates

The reaction for both minerals was faster at higher temperatures, as predicted by thermodynamics and previous studies (Acero et al., 2007; Kimball et al., 2010), and determined by using an Arrhenius plot (Fig. 10). This approach relates the natural log of the specific rate constant to the inverse absolute temperature for fixed concentrations of [H$^+$] and O$_2$. By using Eq. (14), where k is the reaction rate constant, A is the frequency factor, R is the universal gas constant, and T is temperature in kelvin, the activation energies (E$_a$) are calculated to be 40.26 kJ/mol for pyrrhotite and 10.14 kJ/mol for chalcopyrite.

$$k = Ae^{-Ea/RT} \tag{14}$$

6. Discussion

6.1. Effects of individual variables on reaction rates

The observed effects on the reaction rates of these sulfides varied in magnitude and direction for each variable. Higher oxidant concentration increases the reaction rate for both pyrrhotite and chalcopyrite, and the data indicate that the effect of DO on the pyrrhotite reaction rate is nonlinear. The pyrrhotite reaction rate at 0.100 atm was higher than it was at both 0.001 atm and 0.995 atm. However, since there is limited DO at seafloor conditions, it is likely that reaction rates will be most similar to the slowest observed in this study, at the lowest DO concentrations. Therefore, to extrapolate to seafloor conditions, it is most appropriate to use a regression between the two lowest P$_{O2}$ values.

Variations in surface area have a stronger effect, which is important when considering that the seafloor mining process will

either leave behind small particles or discharge them above the seafloor as waste. A strong non-unity effect of varying surface area was observed for pyrrhotite, implying that dissolution at grain edges, corners, cleavages and etch pits may be more important than at the bulk surface (Fig. 9). The dissolution of chalcopyrite was also significantly hindered by decreased surface area (increased grain size). The rate of a chalcopyrite-seawater reaction was essentially rendered undetectable under such conditions, indicating that surface area has an even stronger effect on chalcopyrite. These observations are important because as the main ore mineral of interest (chalcopyrite) and the main gangue mineral (pyrrhotite), fine particles (≤8 μm) of both minerals are likely to be in the waste slurry that is returned to the sea after processing. Despite a lack of data from this study to demonstrate the exact surface area effect on the oxidation of chalcopyrite in seawater, the literature (i.e., Kimball et al., 2010) maintains a prediction of a higher surface area to volume ratio escalating the rate of this reaction.

Contrary to the impacts of oxidant concentration and surface area, the effect of pH on the reaction rate for both pyrrhotite and chalcopyrite is minimal over the range studied, indicated by the comparatively shallow slopes observed in Fig. 6 for both sulfides. This implies that if acidification were to occur at seafloor conditions from natural or anthropogenic causes (low DO, low T), the increasing local acidity will likely not cause a run-away feedback effect in the way of greatly increasing acid production via sulfide oxidation. Thus, since DO and T should remain constant in the seafloor environment, the variable most important to consider in the context of seafloor mining, and the one most affected by the process, is surface area (grain size).

6.2. The range of sulfide oxidation rate in seawater

The rapid rate of pyrrhotite oxidation can be considered an upper limit for sulfide mineral oxidation on the seafloor, while the slow rate of chalcopyrite oxidation can be considered a minimum. The oxidation rates of other sulfides commonly found at hydrothermal vents (e.g., pyrite) should lie within this range. These rates are affected by temperature, surface area, pH, and oxidant concentration. Although the reaction rates are affected positively at low pH by temperature, DO, and surface area, measurements of the reaction rate were afflicted by the formation of precipitates at normal seawater pH. In fact, chalcopyrite releases Cu and Fe so sluggishly at average seawater pH (~8.2), that the dissolution rate was immeasurable, which is encouraging for mining companies looking to exploit deposits principally composed of chalcopyrite and located away from the influence of acidic black smoker plumes: there should be no measurable acid release and no loss of Au-rich ore from oxidative dissolution.

6.3. Buffer capacity of seawater

Since seawater is an excellent buffer for changes in pH, we must also consider how a realistically large volume of it will respond to acid produced via sulfide oxidation. The buffer capacity (B$_c$) is the threshold at which a solution is able to resist changes to pH (Eq. (15)) and is a function of chlorinity (Cl) (Thompson and Bonnar, 1931):

$$Bc/Cl = 0.1252 \tag{15}$$

For average seawater containing about 34 g of salt per kg, including about 19 g of Cl$^-$, the B$_c$ is 2.38 g of acid per kg of seawater. If we assume sulfide reaction with 1 kg of seawater, and if congruent oxidation of chalcopyrite occurs following Rxn. 3, then 1 mol (1.008 g) of H$^+$ is produced. For pyrrhotite, Rxn. 1 shows that
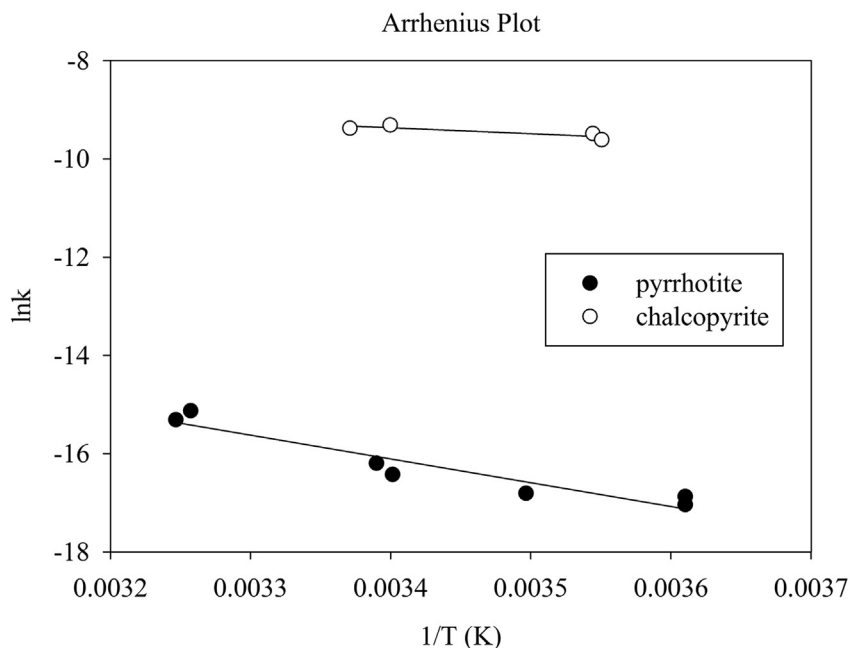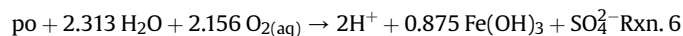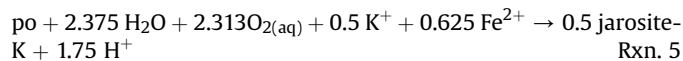
Arrhenius Plot

Fig. 10. Arrhenius plot for pyrrhotite (solid circles) and chalcopyrite (open circles).

dissolution of 1 mol will produce 2 mol of H^+, or 2.016 g of acid. This is well within seawater's buffer capacity, especially factoring in advective effects. It is pertinent to note, though, that anthropogenic reduction of oceanic pH by rising atmospheric CO_2 will accelerate the weathering of SMS deposits as the condition persists; however, the sheer volume of water available will couple with B_c to dilute, disperse, and buffer the acid produced.

6.4. Comparison of experimental results and a Geochemist's workbench model

Although it is possible to predict sulfuric acid production from oxidation by molar relationships alone as we have done above, there are several different possible reactions that could take place on the seafloor. Further, due to the formation of precipitates at higher pH, our experiments only allowed us to investigate the initial rates of these reactions in batch reactors at lower pH conditions where precipitation does not occur. Therefore, we have also modeled the complete stoichiometric oxidation of pyrrhotite at higher pH in order to compare results with our calculations of acid production from Rxn. 1 in section 6.3. We focus on pyrrhotite as it is the faster-oxidizing massive sulfide and a common mining waste product. The following pyrrhotite (po) oxidation reactions were written in terms of these products using GWB:

$$po + 2.375\,H_2O + 2.313\,O_{2(aq)} + 0.5\,K^+ + 0.625\,Fe^{2+} \rightarrow 0.5\,\text{jarosite-}K + 1.75\,H^+ \qquad \text{Rxn. 5}$$

$$po + 2.313\,H_2O + 2.156\,O_{2(aq)} \rightarrow 2H^+ + 0.875\,Fe(OH)_3 + SO_4^{2-} \qquad \text{Rxn. 6}$$

Using the stoichiometry of Rxn. 5, each kg of pyrrhotite reacted produces 2.70 mg of protons. In Rxn. 6, for every kg of pyrrhotite, 3.09 mg of protons are produced.

At pH = 7.5, GWB predicts both Fe hydroxide and jarosite precipitation (Fig. 7). Further, GWB predicts that *total* consumption of pyrrhotite during oxidation in seawater will yield a significant drop in pH (Fig. 8). However, the reactions written with the program using the same reactants do not produce large amounts of protons

when the buffer capacity is calculated by hand. Although molar relationships do not predict enough acid production to drive the local seawater pH down, experiments may not have been run long enough to observe and measure this empirically. The GWB model simulates the complete dissolution of 1 g of sulfide in 1 kg of seawater and is not time-limited. Since a slight increase in pH was observed in pyrrhotite experiments at pH 5 and above, hydroxide production may initially exceed proton production; however, if the reaction were to run to completion proton production would still not exceed hydroxide production by molar predictions. It is also possible that at higher pH, an oxidative coating develops on pyrrhotite grains early on in the reaction preventing further dissolution of Fe and release of protons. This phenomenon has been demonstrated in pyrite (Nicholson et al., 1990) and inferred as a possibility during pyrrhotite oxidation in freshwater (Nicholson and Sharer, 1994).

6.5. Residence time of sulfide grains near mine sites

Additional factors will play a role in acid production from seafloor mining, but were not investigated in this study. For example, the SMS material will be pulverized *in situ* and then slurried up to a mining support vessel on the surface for rough processing (Hoagland et al., 2010). During this time, the material will be further crushed, creating more surface area and exposing fresh, unreacted surfaces. These fresh grain surfaces will then experience both higher temperatures and oxidant concentrations at the surface, variables that accelerate oxidation.

Following shipboard processing, waste effluent containing grains <8 μm in diameter will be piped back to depth and released just above the seafloor (Gwyther and Wright, 2008). The fate of these particulates is akin to that of natural vent particulates produced by active hydrothermal vents, but perhaps in larger quantities. Because acidity and other ecological effects could be produced by these released particulates, we should consider how long they will persist near the seafloor. The "shrinking sphere model" from Hume and Rimstidt (1992) (adapted by Jurinski, 1998) can be used to evaluate how long it would take for a sulfide grain to completely oxidize at the seafloor. The following equation defines the amount

of time (Δt) it takes a spherical grain to completely dissolve under conditions controlled by the specific rate constant (k):

$$\Delta t = d \, / \, 2V_m k \tag{16}$$

where d is the diameter of a spherical grain, V_m is the molar volume. Since this equation was derived for a zeroth order reaction, to adapt for the sulfide oxidations, reaction R_{sp} (mol m^{-2} sec^{-1}) for runs at 23.0 °C and $P_{O2} = 0.10$ were substituted for k and pH was extrapolated to a more realistic value of 8. The time for a pyrrhotite grain of the smallest proposed waste sulfide diameter (8 µm) would take approximately 1.44 months to be completely consumed, while a chalcopyrite grain would last about 6 years and 11 months. Additional values for other grain sizes are reported in Table 1. The actual time would likely be longer than this since these rates are applicable for conditions approximately 20° warmer than seafloor temperature.

6.6. Potential effects of biotic oxidation

Although the effect of bacteria on sulfide oxidation in seawater is currently unknown, bacterial catalysis of oxidation may be insignificant on the timescale of seafloor mining. Therefore, inorganic rates are most relevant to rapid seafloor mining time spans (minutes to days), within which significant bacterial colonization of freshly ground sulfide mineral surfaces is not likely to occur (e.g., McBeth et al., 2011). Advective and diffusive transport of ocean currents also contributes to the sphere of influence of mining activities on the seafloor.

7. Future work

There is an abundance of further work required to fully understand the impending effects of seafloor mining, much of which is outside of the scope of abiotic kinetics research. However, there are also opportunities to expand upon this type of study, such as employing flow-through reactors to avoid the formation of precipitates during experiments in order to collect data at pH conditions closer to the seawater present at unmined inactive hydrothermal vents. Several flow-through experiments were run with pyrrhotite but time did not permit for an entire flow-through study. Rate laws also need to be developed for other common SMS minerals (e.g., pyrite, galena, sphalerite) as well as sulfate minerals formed at white smokers (e.g., gypsum, anhydrite). A study of bacterial catalysis would also provide more information on the potential effects of sulfide mineral oxidation on seafloor ecology.

Additionally, when rate laws are incorporated into reactive transport computer models, they may be able to predict how long Fe sulfide particles in both natural vent plumes and anthropogenic mining discharge plumes might persist. Some modeling has been done to mix hydrothermal fluids from black smokers with seawater, simulating mineral precipitation near seafloor vents (Janecky and Seyfried, 1984). Thermodynamic data and reaction modeling codes could be accommodated to mining activity to predict the nature and persistence of waste material. This industry is developing rapidly due to the demand and high price of Cu and Au, however it is imperative that we are able to identify and control the effects on the environment and biota that live at and near the vents.

8. Conclusions

The results presented here are useful to quantify the natural and anthropogenic weathering rates of SMS deposits. As the seafloor mining industry develops due to metal demand, it is important that we are able to identify and control the effects on the environment. While unanswered questions remain, these new data on the kinetics of abiotic sulfide oxidation in seawater allow us to draw the following conclusions:

1. At low pH, the abiotic oxidation rate of both pyrrhotite and chalcopyrite in seawater is affected positively by increasing H$^+$ concentration, temperature, surface area, and P_{O2}.
2. The rate of oxidation for pyrrhotite is most significantly affected by temperature and oxidant concentration.
3. The rate of oxidation of chalcopyrite in seawater is slower than that of pyrrhotite and more dependent on P_{O2} than pH, but the reaction can occur more than an order of magnitude faster at pH 2.2 than at pH 4.5.
4. Anthropogenic ocean acidification due to CO_2 would have to produce unrealistically low pH values (<4.5) to significantly accelerate the weathering of SMS deposits.
5. Above pH 4.5, sulfide mineral dissolution is hindered by the production of precipitates and therefore not covered in this batch mode study.
6. The rate of the pyrrhotite oxidation reaction can be considered an upper limit for sulfide oxidation on the seafloor, while chalcopyrite oxidation bounds the lower limit.
7. Acid produced by the abiotic oxidation of both pyrrhotite and chalcopyrite during the timeframe of mining may be naturally buffered by advecting seawater.
8. Persistence times of small grains of these sulfides (<10 µm) generated in the effluent of mining activities can be up to several years, implying that ecological concerns should focus more on the physical impact of the particulates themselves, rather than any acidity that may be produced from their mining and dissolution.

In summary, the overall implications of these first kinetic experiments show that it is possible that *significant* seafloor AMD will not occur from mining activities. Although computer modeling (GWB) predicts a significant pH drop, the complete oxidative dissolution of sulfide minerals is not actually occurring in reality, even at low pH. Both the experimentally derived rates of reactions and the acid production calculated from simple reaction stoichiometry support the conclusion that the actual acid production will be limited and likely not exceed the buffer capacity of seawater. Physical impacts caused by released particles (e.g., suffocation of benthic organisms) may therefore be more significant than chemical impacts.

Table 1
Grain lifetime (Δt) at $P_{O2} = 0.10$ atm, pH = 8, T = 23 °C.

Diameter:	1 µm	8 µm	10 µm
$\Delta t_{pyrrhotite}$ (years):	0.02	0.16	2.04
$\Delta t_{chalcopyrite}$ (years):	0.87	6.93	86.62

References

Acero, P., Cama, J., Ayora, C., 2007. Kinetics of chalcopyrite dissolution at pH 3. Eur. J. Mineral. 19, 173–182.

Avery, E.R., Benning, L.G., 2008. Direct vs. Indirect Quantification of Pyrite Oxidation Rates, A38. Goldschmidt Conference Abstracts, Vancouver.

Baker, E., Beaudoin, Y., 2013. Environmental management considerations, deep sea minerals: sea-floor massive sulphides. In: A Physical, Biological, Environmental, and Technical Review, vol. 1A. Secretariat of the Pacific Community.

Becker, H.E.K., Davis, E.E., 2004. Foundations of research into heat, fluid, and chemical fluxes in oceanic crust. Hydrogeol. Ocean. Lithosphere CD-ROM 1, 28.

Belzile, N., Chen, Y.-W., Cai, M.-F., Li, Y., 2004. A review on pyrrhotite oxidation. J. Geochem. Expl. 84, 65–76.

Benson, B.B., Krause, D., 1980. The concentration and isotopic fractionation of gases dissolved in freshwater in equilibrium with the atmosphere. 1. Oxygen. Limonl. Oceanogr. 95, 662–671.

Benson, B.B., Krause, D., 1984. The concentration and isotopic fractionation of oxygen dissolved in freshwater and seawater in equilibrium with the atmosphere. Limonol. Oceanogr. 29, 620–632.

Bethke, C.M., 2008. Geochemical and Biogeochemical Reaction Modeling, second ed. Cambridge Univ. Press, N.Y. 543 pp.

Bilenker, L.D., 2011. Abiotic Oxidation Rate of Chalcopyrite in Seawater: implications for Seafloor Mining. M.Sc. Thesis. University of California, Riverside.

Blodau, C., 2006. A review of acidity generation and consumption in acidic coal mine lakes and their watersheds. Sci. Total Environ. 369, 307–332.

Boschen, R.E., Rowden, A.A., Clark, M.R., Gardner, J.P.A., 2013. Mining of deep-sea seafloor massive sulfides: a review of the deposits, their benthis communities, impacts from mining, regulatory frameworks and management strategies. Ocean. Coast. Manage. 84, 54–67.

Brunauer, S., Emmett, P.H., Teller, E., 1938. Adsorption of gases in multimolecular layers. J. Am. Chem. Soc. 60, 309–319.

Brantley, S.L., Kubicki, J.D., White, A.F., 2008. Kinetics of Water Rock Interaction. Springer Science + Business Media, LLC.

Craw, A., 2013. Deep Seabed Mining: an Urgent Wake-up Call to Protect Our Oceans. Greenpeace International, Amsterdam. Report JN 452, 20 pp.

Coffey Natural Systems Pty Ltd, 2008. Environmental impact statement, Solwara 1 project. Naut. Miner. Niugini 1–16.

Davis, E.E., Elderfield, H., 2004. Hydrogeology of the Oceanic Lithosphere. Cambridge University Press, pp. 225–265.

Davis, E.E., Mottl, M.J., Fisher, A.T., et al., 1992. Proceedings ODP. Initial Reports 139.

Drew, L.W., 2009. The promise and perils of seafloor mining. Oceanus 47.

Duckworth, J.R.H., 1998. Drilling of Sediment Hosted Massive Sulphide Deposits at the Middlevalley and Escanaba Trough Spreading Centers. valley and escanaba trough spreading centers. ODP Leg 169. Modern Ocean Floor Processes and the Geologic Record.

Edwards, K.J., McCollum, T.M., Konishi, H., Busek, P.R., 2003. Seafloor bioalteration of sulfide minerals: results from in situ incubation studies. Geochim. Cosmochim. Acta 67, 2843–2856.

Fagurland, G., 1973. Determination of specific surface by the BET method. Mater. Struct. 6, 239–245.

Fornari, D.J., Embly, R.W., 1995. Tectonic and volcanic controls on hydrothermal processes at the mid-ocean ridge: an overview based on near-bottom and submersible studies. AGU 1–46.

Garcia, H.E., Gordon, L.I., 1992. Oxygen solubility in seawater: better fitting equations. Limnol. Ocean. 37, 1307–1312.

Gwyther, D., Wright, M., 2008. Environmental Impact Statement: Solwara 1. Coffey Natural Systems Pty Ltd, pp. 47–65.

Halfar, J., Fujita, R.M., 2002. Precautionary management of deep-sea mining. Mar. Pol. 26, 103–106.

Halfar, J., Fujita, R.M., 2007. Ecology: danger of deep-sea mining. Science 316, 987.

Hannington, M.D., 1993. The formation of atacamite during weathering of sulfides on the modern seafloor. Can. Mineral. 31, 945–956.

Hannington, M.D., deRonde, C.E.J., Petersen, S., 2005. Sea-floor tectonics and submarine hydrothermal systems. Econ. Geol. 100, 111–141.

Heilig, G.K., Gerland, P., Andreecv, K., Li, N., Gu, D., Spoorenberg, T., Ravinuthala, S., Yamarthy, C., Koshy, N., 2012. Population Estimates and Projection Section: Work Program, Outputs, Challenges, Uncertainties. UN Dept. Economic and Social Affairs.

Hoagland, P., Beaulieu, S., Tivey, M.A., Eggert, R.G., German, C., Glowka, L., Lin, J., 2010. Deep-sea mining of seafloor massive sulfides. Mar. Pol. 34, 728–732.

Hoffert, J.R., 1947. Acid mine drainage. Ind. Eng. Chem. 39, 642–646.

Hrischeva, E., Scott, S.D., 2007. Geochemistry and morphology of metalliferous sediments and oxyhydroxides from the Endeavour segment, Juan de Fuca Ridge. Geochim. Cosmochim. Acta 71, 3476–3497.

Hume, L.A., Rimstidt, J.D., 1992. The biodurability of chrysotile asbestos. Am. Mineral. 77, 1125–1128.

International Marine Minerals Society, 2011. Code for Environmental Management of Marine Mining, 15 pp.

International Seabed Authority, 2013. Consolidated Regulations and Recommendations on Prospecting and Exploration. Report 13-40403, 214 pp..

Janecky, D.R., Seyfried, W.E., 1984. Formation of massive sulfide deposits on oceanic ridge crests: incremental reaction models for mixing between hydrothermal solutions and seawater. Geochim. Cosmochim. Acta 48, 2723–2738.

Janzen, M.P., Nicholson, R.V., Sharer, J.M., 2000. Pyrrhotite reaction kinetics: reaction rates for oxidation by O2, Fe3+, and non-oxidative dissolution. Geochim. Cosmochim. Acta 64, 1511–1522.

Johnson, D.B., 2003. Chemical and microbiological characteristics of mineral spoils and drainage waters at abandoned coal and metal mines. Water Air Soil Pollut. 3, 47–66.

Jurinski, J.B., 1998. Geochemical Investigations of Respirable Particulate Matter. Ph.D. thesis. Virginia Polytechnic Institute.

Kim, A.G., Heisey, B.S., Kleinmann, R.L.P., Deul, M., 1982. Acid Mine Drainage: Control and Abatement Research. Series: Information circular (United States. Bureau of Mines), No. 8905, pp. 1–22.

Kimball, B.E., Rimstidt, J.D., Brantley, S.L., 2010. Chalcopyrite dissolution rate laws. Appl. Geochem. 25, 972–983.

Kimball, B.E., 2013. Minerals explained 53: chalcopyrite–bearer of a precious, non-precious metal. Geol. Today 29, 30–35.

Laidler, K.J., 1987. Chemical Kinetics, third ed. Harper Collins.

Lasaga, A.C., 1998. Kinetic Theory in the Earth Sciences. Princeton University Press.

Lu, Z.Y., Jeffrey, M.I., Lawson, F., 2000. The effect of chloride ions on the dissolution of chalcopyrite in acidic solutions. Hydrometallurgy 56, 189–202.

McBeth, J.M., Little, B.J., Ray, R.I., Farrar, K.M., Emerson, D., 2011. Neutrophilic iron-oxidizing "Zetaproteobacteria" and mild steel corrosion in nearshore marine environments. Appl. Envir. Microbio. 77, 1405–1412.

McKibben, M.A., Barnes, H.L., 1986. Oxidation of pyrite in low temperature acidic solutions: rate laws and surface textures. Geochim. Cosmochem. Acta 50, 1509–1520.

McKibben, M.A., Tallant, B.A., del Angel, J.K., 2008. Kinetics of inorganic arsenopyrite oxidation in acidic aqueous solutions. Appl. Geochem 23, 121–135.

Millero, F.J., 2002. Chemical Oceanography. CRC Press LLC, Boca Raton.

Mills, R.A., Elderfield, H., 1995. Hydrothermal activity and the geochemistry of metalliferous sediment. AGU Geophys. Monogr. 91, 392–407.

Mills, R.A., 1995. Hydrothermal deposits and metalliferous sediments from TAG, 26°N Mid-Atlantic Ridge. Hydrothermal Vents Process. Geol. Soc. Special Publ. 87, 121–132.

Nicholson, R.V., Sharer, J.M., 1994. Lab studies of pyrrhotite oxidation kinetics, environmental geochemistry of sulfide oxidation. ACS Symp. Ser. 550, 14–30.

Nicholson, R.V., Gillham, R.W., Reardon, E.J., 1990. Reactivity of the (100) plane of pyrite in oxidizing gaseous and aqueous environments: effects of surface imperfections. Geochim. Cosmochim. Acta 54, 395–402.

Polz, M.F., Robinson, J.J., Cavanaugh, C.M., Van Dover, C.L., 1998. Trophic ecology of massive shrimp aggregations at a Mid-Atlantic Ridge hydrothermal vent site. Limnol. Ocean. 43, 1631–1638.

Pratt, A.R., Muir, I.J., Nesbitt, H.W., 1994. X-ray photoelectron and Auger electron spectroscopic studies of pyrrhotite and mechanism of air oxidation. Geochim. Cosmochim. Acta 58, 827–841.

Rimstidt, J.D., 2014. Geochemical Rate Models.

Romano, G.Y., 2012. Kinetics of Pyrrhotite Oxidation in Seawater: implications for Mining Seafloor Hotsprings. M.Sc. thesis. University of California, Riverside.

Rona, P.A., 2008. The changing vision of marine minerals;. Ore Geol. Rev. 33, 618–666.

Ruiz, M.C., Montes, K.S., Padilla, R., 2011. Chalcopyrite leaching in sulfate-chloride media at ambient pressure. Hydrometallurgy 109, 37–42.

Sasaki, K., Nakamuta, Y., Hirajima, T., Tuovinen, O.H., 2009. Raman characterization of secondary minerals formed during chalcopyrite leaching with Acid-ithiobacillus ferrooxidans. Hydrometallurgy 95, 153–158.

Schippers, A., 2004. Biogeochemistry of Metal Sulfide Oxidation in Mining Environments, Sediments and Soils. Special Paper 379. Geological Society of America, pp. 49–62.

Spiess, F.N., Macdonald, K.C., Atwater, T., Ballard, R., Carranza, A., Cordoba, D., Cox, C., Diaz Garcia, V.M., Francheteau, J., Guerrero, J., Hawkins, J., Haymon, R., Hessler, R., Juteau, T., Kastner, M., Larson, R., Luyendyk, B., Macdougall, J.D., Miller, S., Normark, W., Orcutt, J., Rangin, C., 1980. East pacific rise: hot springs and geophysical experiments. Science 207, 1421–1433.

Thompson, T.G., Bonnar, R.U., 1931. The buffer capacity of sea water. Ind. Eng. Chem. Anal. Ed. 3, 393–395.

Van Dover, C.L., Fry, B., Grassle, J.F., Humphris, S., Rona, P.A., 1988. Feeding biology of the shrimp Rimicaris exoculata at hydrothermal vents on the Mid-Atlantic Ridge. Mar. Biol. 98, 206–216.

Van Dover, C.L., 2011. Mining seafloor massive sulphides and biodiversity: what is at risk? ICES J. Mar. Sci. 68, 341–348.

Von Damm, K.L., 1995. Controls of the Chemistry and Temporal Variability of Seafloor Hydrothermal Fluids. Seafloor Hydrothermal Systems: Physical, Chemical, Biological, and Geological Interactions. American Geophysical Union.

Yeats, C.J., Parr, J.M., Binns, R.A., Gemmell, J.B., Scott, S.D., 2014. The SuSu knolls hydrothermal field, eastern manus basin, Papua New Guinea: an active submarine high-sulfidation copper-gold system. Econ. Geol. 109, 2207–2226.